Available online at www.sciencedirect.com
ScienceDirect
Geochimica et Cosmochimica Acta 73 (2009) 1841–1856
Geochimica et Cosmochimica Acta
www.elsevier.com/locate/gca

Inner-sphere complexation of cations at the rutile–water interface: A concise surface structural interpretation with the CD and MUSIC model

Moira K. Ridley [a,*], Tjisse Hiemstra [b], Willem H. van Riemsdijk [b], Michael L. Machesky [c]

[a] Department of Geosciences, Texas Tech University, Lubbock, TX 79409-1053, USA
[b] Department of Soil Quality, Wageningen University, P.O. Box 8005, 6700 EC Wageningen, The Netherlands
[c] Illinois State Water Survey, 2204 Griffith Drive, Champaign, IL 61820, USA

Received 17 March 2008; accepted in revised form 14 January 2009; available online 22 January 2009

Abstract

Acid–base reactivity and ion-interaction between mineral surfaces and aqueous solutions is most frequently investigated at the macroscopic scale as a function of pH. Experimental data are then rationalized by a variety of surface complexation models. These models are thermodynamically based which in principle does not require a molecular picture. The models are typically calibrated to relatively simple solid-electrolyte solution pairs and may provide poor descriptions of complex multi-component mineral–aqueous solutions, including those found in natural environments. Surface complexation models may be improved by incorporating molecular-scale surface structural information to constrain the modeling efforts. Here, we apply a concise, molecularly-constrained surface complexation model to a diverse suite of surface titration data for rutile and thereby begin to address the complexity of multi-component systems. Primary surface charging curves in NaCl, KCl, and RbCl electrolyte media were fit simultaneously using a charge distribution (CD) and multisite complexation (MUSIC) model [Hiemstra T. and Van Riemsdijk W. H. (1996) A surface structural approach to ion adsorption: the charge distribution (CD) model. *J. Colloid Interf. Sci.* **179**, 488–508], coupled with a Basic Stern layer description of the electric double layer. In addition, data for the specific interaction of Ca^{2+} and Sr^{2+} with rutile, in NaCl and RbCl media, were modeled. In recent developments, spectroscopy, quantum calculations, and molecular simulations have shown that electrolyte and divalent cations are principally adsorbed in various inner-sphere configurations on the rutile 1 1 0 surface [Zhang Z., Fenter P., Cheng L., Sturchio N. C., Bedzyk M. J., Předota M., Bandura A., Kubicki J., Lvov S. N., Cummings P. T., Chialvo A. A., Ridley M. K., Bénézeth P., Anovitz L., Palmer D. A., Machesky M. L. and Wesolowski D. J. (2004) Ion adsorption at the rutile–water interface: linking molecular and macroscopic properties. *Langmuir* **20**, 4954–4969]. Our CD modeling results are consistent with these adsorbed configurations provided adsorbed cation charge is allowed to be distributed between the surface (0-plane) and Stern plane (1-plane). Additionally, a complete description of our titration data required inclusion of outer-sphere binding, principally for Cl^- which was common to all solutions, but also for Rb^+ and K^+. These outer-sphere species were treated as point charges positioned at the Stern layer, and hence determined the Stern layer capacitance value. The modeling results demonstrate that a multi-component suite of experimental data can be successfully rationalized within a CD and MUSIC model using a Stern-based description of the EDL. Furthermore, the fitted CD values of the various inner-sphere complexes of the mono- and divalent ions can be linked to the microscopic structure of the surface complexes and other data found by spectroscopy as well as molecular dynamics (MD). For the Na^+ ion, the fitted CD value points to the presence of bidenate inner-sphere complexation as suggested by a recent MD study. Moreover, its MD dominance quantitatively agrees with the CD model prediction. For Rb^+, the presence of a tetradentate complex, as found by spectroscopy, agreed well with the fitted CD and its predicted presence was quantitatively in very good agreement with the amount found by spectroscopy.

* Corresponding author. Fax: +1 806 742 0100.
E-mail address: moira.ridley@ttu.edu (M.K. Ridley).

0016-7037/$ - see front matter © 2009 Elsevier Ltd. All rights reserved.
doi:10.1016/j.gca.2009.01.004

1. INTRODUCTION

The interface between minerals and aqueous solutions is one of the most complex and fundamentally important geochemical regimes. The distinct properties and chemical reactivity of the interface domain arises from the chemical and physical differences of mineral surfaces from the same material in the bulk. Acid–base reactivity between mineral surfaces and aqueous solutions impart a pH-dependent surface charge that must be balanced by ionic countercharge in the interface. The acid–base reactivity primarily involves protonation and deprotonation of various surface functional groups at the mineral surface. The extent of mineral surface charging results from the chemical and electrostatic interactions with water, counter- and co-ion interactions, and determines the specific adsorption of ions, collectively giving rise to an interface domain termed the electrical double layer (EDL).

The complex interactions taking place at mineral-solution interfaces have been investigated extensively through experimental and theoretical studies. Ion adsorption and surface charging have been studied most frequently as a function of pH, at the macroscopic scale (Davis and Leckie, 1978; Davis et al., 1978; Dzombak and Morel, 1990; Boily and Fein, 1996; Boily et al., 2000; Wesolowski et al., 2000; Ridley et al., 2005; Machesky et al., 2006; Stachowicz et al., 2006). The resulting data have typically been rationalized by various surface complexation models (SCM), which combine chemical descriptions of surface protonation and ion adsorption reactions with electrostatic descriptions of the EDL (Westall and Hohl, 1980; Dzombak and Morel, 1990; Venema et al., 1996a). However, numerous shortcomings of these techniques and models have been identified. A principal shortcoming is that macroscopic experimental data alone cannot provide unambiguous information on microscopic (atomic) level structures (e.g., Westall and Hohl, 1980). Consequently, the numerical fitting parameters of SCM's frequently are poorly constrained, and the electrostatic parameters and equilibrium constants may be highly covariant.

Molecular-scale surface structural information of the interaction of water and ion adsorption at metal-oxide surfaces, such as TiO_2 and various Fe(hydr)oxides, is available from in situ small-period X-ray standing wave measurements (Fenter et al., 2000, 2002, and references therein), grazing-incidence X-ray absorption (GI-XAF) spectroscopy (Towle et al., 1999a,b), and EXAFS (Axe et al., 1998; Ragnarsdottir et al., 1998; Brown et al., 1999; Sahai et al., 2000). Measurements with these techniques reveal precise structural information on the coordination geometry of specifically adsorbed ions. Similarly, crystal truncation rod analysis provides information on the height of adsorbed ions above crystal surface planes (Fenter et al., 2002; Zhang et al., 2004; Zhang et al., 2006, and references therein). However, X-ray techniques also have limitations. For example, measurements of elements with atomic numbers less than about 19 are difficult and this range includes common natural electrolyte ions (Na^+, Cl^-), as well as H^+ (Brown and Sturchio, 2002). Additional constraints of in situ X-ray measurements are the limited range of solution compositions that can be studied within available beam time, and possible damage from the X-ray beam itself.

Surface complexation models are powerful tools to scale from the molecular to the macroscopic scale, provided that molecular-scale surface structural information can be incorporated into the models. The "Classical SCMs" relied on hypothetical surface species, such as the generic 2-pK surface protonation scheme (Parks and De Bruyn, 1962; Berube and De Bruyn, 1968) that did not incorporate any surface structural information for the minerals of interest. However, the revised multisite surface complexation (MUSIC) model (Hiemstra et al., 1989, 1996; Machesky et al., 2001) permits the incorporation of molecular-scale surface structural information into a thermodynamic modeling framework. The MUSIC model considers specific surface functional groups known to exist on individual crystallographic faces exposed on mineral surfaces. Charge attribution and proton affinity constants, pK_a values, are estimated based on bond valence principles and account for variation in metal–oxygen (M–O) bond lengths (Brown and Altermatt, 1985; Brown, 2002). The latter is important as relaxed surface structures at crystal faces can result in M–O bond lengths differing from bulk values. Hydrogen bond interactions with associated H_2O molecules, as can be extracted from classical- and quantum molecular dynamics simulations are also included in recent extensions of the revised MUSIC model (Machesky et al., 2008). In the case of rutile, the focus of this contribution, surface- and H-bond lengths have been determined by *ab initio*, quantum- and molecular dynamic simulations specifically targeting Ti—O bonds of the rutile (1 1 0) surface (Zhang et al., 2004; Fitts et al., 2005). Moreover, the (1 1 0) surface dominates the specific rutile powder used in the experimental studies presented here (Ridley et al., 2002). Theoretical simulations also provide molecular-scale details of the EDL structure, including the structure of electrolyte solutions, and the coordination geometry of specifically adsorbed ions at the rutile (1 1 0) surface (Předota et al., 2004a,b; Předota and Vlček, 2007a,b; Vlček et al., 2007; Zhang et al., 2007).

Earlier studies have provided significant insights into ion adsorption and the interface domain (for example, Venema et al., 1996b; Bourikas et al., 2001; Rietra et al., 2001; Ridley et al., 2004, 2005; Zhang et al., 2004; Sverjensky, 2005; Boily et al., 2005; Fitts et al., 2005; Hiemstra and Van Riemsdijk, 2006; Machesky et al., 2006). In general, systems with electrolyte ions have been described with rather simple EDL models. The adsorption of so-called "inert electrolyte" ions are typically treated as being exclusively non-specific and outer-sphere. However, X-ray spectroscopy has revealed that electrolyte cations can form inner-sphere complexes at the (1 1 0) face of rutile (Fenter et al., 2000; Zhang et al., 2004, 2007). Moreover, the observed structures have been incorporated into a few previous modeling efforts (Zhang et al., 2004; Ridley et al., 2005). In these prior efforts, however, electrolyte cations have been considered as simple point charges. The question, therefore, arises as to whether the Charge Distribution (CD) approach of Hiemstra and Van Riemsdijk (1996) can also be applied, while also con-

forming to bonding geometries identified via X-ray and computational methods. Within the CD model, an inner-sphere bound ion contributes partly to the neutralization of the surface ligands. For this reason, part of the ion charge is attributed to the surface and the remaining part is attributed to the free ligands and located at some distance from the surface (i.e. a Stern plane), in a manner that is predictable from the structure of the adsorbed ion.

In this contribution, we continue to build on the application of the CD and MUSIC model to provide a mechanistically accurate and thermodynamically rigorous description of macroscopic ion-adsorption data for rutile. Primary titration curves have been determined in NaCl, KCl, and RbCl electrolyte media at various concentrations, and additionally the interaction of $CaCl_2$ and $SrCl_2$ in these media have been measured. This comprehensive data set provides an opportunity to start to address the complexity of multi-component systems while utilizing microscopic information.

All 1:1 electrolyte data were interpreted with the CD and MUSIC model (Hiemstra and Van Riemsdijk, 1996). The assumption is that ions may be present in the compact part of the double layer as inner-sphere and/or outer-sphere complexes or in the diffuse double layer. A basic principle is that counterions have a finite size with a corresponding minimum distance of approach to the mineral surface (Stern, 1924); consequently, each electrolyte ion has a unique position within the EDL, which will affect the CD value and the capacitance of the Stern layer. Both are needed for a consistent description of the data. The approach taken in fitting the divalent ions was to keep constant all model parameters resulting from fitting the monovalent electrolyte ion data, i.e. the same Basic Stern layer description of the EDL and the CD–MUSIC model approach. This modeling framework reduces the overall number of fitting parameters. Moreover, the model parameters are applicable to a wider range of solution compositions, consistent with multi-component solutions that may be encountered in natural systems. In all SCM fitting endeavors available molecular-scale X-ray synchrotron measurements, and *ab initio* and MD simulation results were used to help constrain the fitting parameters.

2. EXPERIMENTAL

The rutile powder used in this study was from Tioxide Corporation and has been used extensively in previous studies (Machesky et al., 1994, 1998; Ridley et al., 2002, 2005). The specific N_2-BET surface area was 14.4 ± 0.1 m^2/g (after hydrothermal pretreatment following Machesky et al. (1998)), which is slightly lower than the batch used in some of our previous studies (17 ± 2 m^2/g). The primary particles were needle-shaped, approximately 500 nm long and 50 nm wide, as observed by Scanning Electron Microscopy (SEM) (Ridley et al., 2002). All experimental solutions were prepared from reagent-grade chemicals and deionized water. The general method used to prepare and store these solutions has been described previously (Ridley et al., 1998a,b, 1999a; Wesolowski et al., 2000). All solutions were prepared at ionic strengths of 0.03 and 0.3 m total molalities (where m is used throughout this paper to indicate aqueous concentration in units of molality, moles of solute per kilogram of water). To obtain primary proton adsorption curves, solutions were prepared from NaCl, KCl and RbCl. For all experiments, the initial electrode calibration solution was basic, comprising 5×10^{-4} m OH^- (see potentiometric titration procedure below), to which an acid calibration solution was added that contained sufficient HCl to attain a calibration point close to 0.002 m H^+. These calibration solutions contained sufficient electrolyte to produce the desired ionic strength (Ridley et al., 2002). The test solutions for determining the adsorption behavior of rutile in the presence of Ca^{2+} and Sr^{2+} ions comprised 0.001 m Ca^{2+} or Sr^{2+}, 0.002 m H^+ and sufficient NaCl or RbCl to produce the desired ionic strength. The adsorption of Ca^{2+} was determined in NaCl media, whereas titrations of Sr^{2+} adsorption were completed in both NaCl and RbCl media. The titrant solutions comprised OH^- and the electrolyte media of interest; as in previous studies (Ridley et al., 1999a, 2002, 2005) the ionic strength of the titrant was slightly higher than the corresponding test solution, making it possible to largely compensate for changes in ionic strength during a titration. Consequently, the ionic strength varied no more than 3% throughout a particular titration. Furthermore, data reduction of the potentiometric titrations accounted for all dilution effects (Ridley et al., 2006).

The experimental system and equipment used in this study, and the potentiometric titration procedures have been discussed in detail by Machesky et al. (2006) and Ridley et al. (2002, 2006). For all potentiometric titrations a Mettler DL70 autotitrator and Ross Semimicro combination glass-electrodes were utilized. In each titration, 1 g of rutile was suspended in 40 g of test solution. The titration cell was immersed in a water bath at 25 °C (±0.1 °C), the headspace was purged with purified argon to prevent CO_2 contamination; and the solutions were stirred mechanically at all times. During each titration 20–30 aliquots of titrant were added, over a pH_m range of approximately 8 units. The titrations were terminated when the measured cell potential exceeded the calibration range. For each point in the titrations, the net proton adsorption (desorption) expressed as an excess or deficit of micromoles H^+ per square meter of mineral surface, were obtained. In addition, a second set of independent adsorption titrations were completed for Sr^{2+}. The second set, referred to as adsorption 'pH-edge' experiments (Dzombak and Morel, 1990), consisted of titrations during which samples were periodically withdrawn from the test solution. The withdrawn sample aliquots were filtered through 0.2 μm filters into preweighed polypropylene syringes containing a known amount of high purity 1 m HNO_3 for later analysis of the total dissolved Sr concentration by ICP.

3. EXPERIMENTAL RESULTS

3.1. Primary electrolyte proton adsorption curves

The net proton adsorption curves (expressed as excess/deficit μmols H^+/m^2) of rutile in each background electro-

lyte (NaCl, KCl and RbCl) are shown in Fig. 1. Standard deviation of the μmols H^+/m^2 values was determined from replicate titration data, with one standard deviation being smaller than the data symbols shown in Fig. 1. For each electrolyte, the titrations at 0.03 and 0.3 m exhibit a common intersection point (CIP) at a pH of 5.4, that corresponds closely to zero μmols H^+/m^2 obtained from H^+ mass balance calculations. Consequently, as in our previous studies (Machesky et al., 1994, 1998; Ridley et al., 1999b, 2002), this intersection point defines the zero net proton charge value (pH_{znpc}). Moreover, the pH_{znpc} is identical to that obtained with our previous batch of Tioxide rutile and is unaffected by the type of 1:1 electrolyte cation, suggesting that the interaction of cations and anions with the surface is quite similar or weak near the pH_{znpc}. This also follows from the almost identical charging curve in different electrolytes at low electrolyte concentrations as is shown in Fig. 2. At low ionic strength, 0.03 m, the slopes of the titration curves are similar for the three cations (Fig. 2a), meaning they screen negative surface charge development similarly. However, at 0.3 m ionic strength and higher pH the slopes of the titration curves vary with the cation (Fig. 2b), indicating enhanced screening in the order $Na^+ > K^+ > Rb^+$. Similarly, Berube and De Bruyn (1968) reported that Na^+ resulted in a greater negative surface charge development on rutile than did K^+. This trend was also found by Bourikas et al. (2001) in their examination of the charging behavior of a large number of Ti oxides.

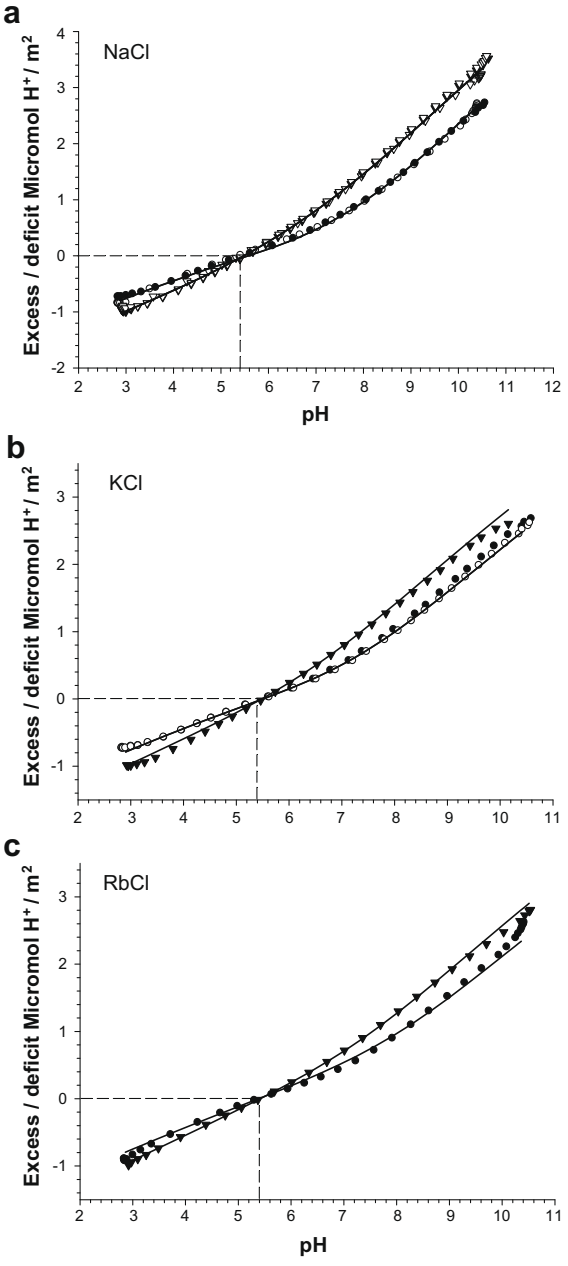

Fig. 1. The relative proton adsorption/desorption on rutile in each background electrolyte media is shown. All curves represent the CD–MUSIC model fits. The model parameter values are defined in the text and given in Table 1. The symbols represent experimental data at ionic strengths of 0.03 (●) or 0.3 m (▼), and the open or closed symbols illustrate multiple titrations. One standard deviation of the μmols H^+/m^2 values, determined from the replicate titrations, is smaller than the data symbols. The dashed vertical and horizontal lines represent the pH_{znpc} value and the zero surface charge value, respectively.

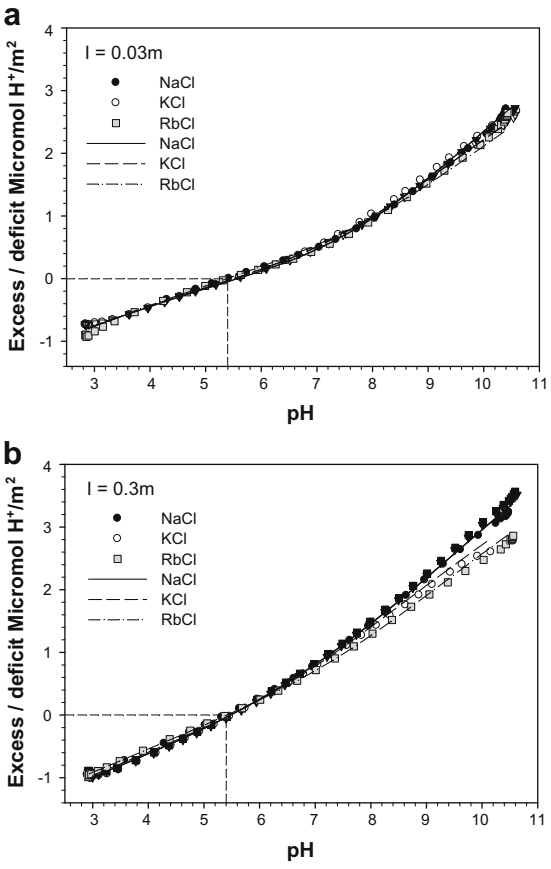

Fig. 2. Titration data showing the effect of electrolyte cation type on the relative proton adsorption/desorption at ionic strengths of 0.03 or 0.3 m. All curves represent the CD–MUSIC model fits. The model parameter values are defined in the text and given in Table 1. The dashed vertical and horizontal lines represent the pH_{znpc} value and the zero surface charge value, respectively.

Increased screening can result from a greater intrinsic affinity (larger binding constant) and/or a closer approach to the surface. In the case of rutile, proton desorption (or equivalent OH^- adsorption) from the rutile surface increases with decreasing bare crystallographic radii of the cations (1.49, 1.38 and 1.02 Å for Rb^+, K^+, and Na^+, respectively (Marcus, 1997)). This inverse lyotrophic sequence has been interpreted by Sverjensky (2001, 2005) to result both from larger binding constants and a closer approach of ions to the surface of minerals with high bulk dielectric constants, such as rutile.

3.2. Adsorption of divalent cations

The presence of divalent cations (i.e., Ca^{2+} and Sr^{2+}) strongly enhances proton desorption (or equivalent OH^- adsorption) at the rutile surface (Fig. 3). As reported previously by Ridley et al. (1999a, 2004), the adsorption of Ca^{2+} and Sr^{2+} to the rutile surface commences at pH values near the pH_{znpc}; whereas other authors have reported a decrease in the apparent pH_{znpc} values for divalent cation adsorption from low ionic strength solutions (for example, (Jang and Fuerstenau, 1986)). At high pH (>8) the excess of H^+ in solution was slightly greater in the presence of Ca^{2+} than Sr^{2+} (Fig. 3), as might be expected from the smaller bare crystallographic radius of Ca^{2+}. Indeed, classical MD simulations (Předota et al., 2004b; Předota and Vlček, 2007b) find Ca^{2+} adsorbed in tetradentate fashion is about 0.2 Å closer to the rutile surface than is Sr^{2+}. In addition, the amount of specifically adsorbed Ca^{2+} may be slightly higher ($\Gamma_{Ca} > \Gamma_{Sr}$, μmol/m^2), and this greater Ca^{2+} adsorption would increase H^+ desorption relative to that for Sr^{2+}.

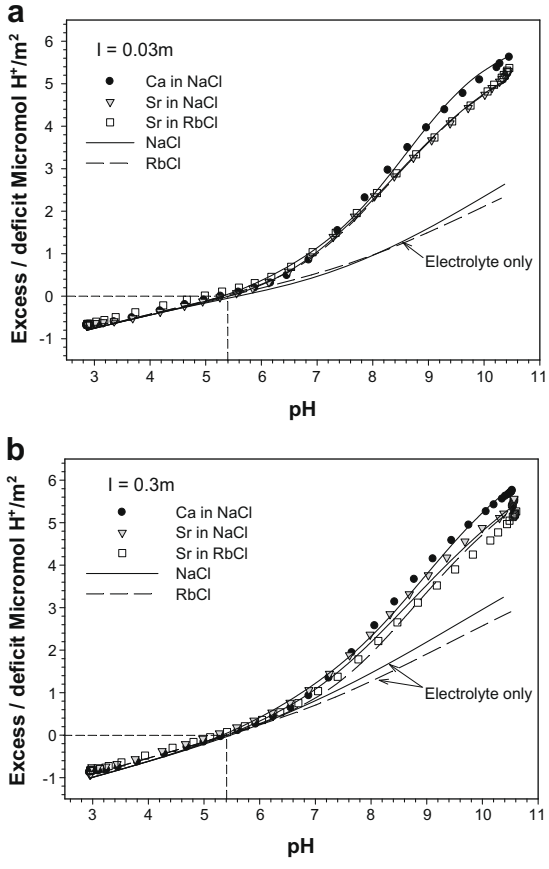

Fig. 3. The relationship between the relative proton adsorption/desorption of rutile for titrations performed in NaCl and/ or RbCl electrolyte solutions in the presence or absence of Ca^{2+} and Sr^{2+}. The symbols represent experimental data in the presence of Ca^{2+} or Sr^{2+}. All curves represent the CD–MUSIC model fits, in NaCl (solid lines) and RbCl (dashed lines) media. The model parameter values are defined in the text and given in Table 1. The dashed vertical and horizontal lines represent the pH_{znpc} value and the zero surface charge value, respectively.

At low ionic strength (0.03 m), H^+ desorption in the presence of Sr^{2+} was unaffected by the type of monovalent electrolyte cation (i.e., Na^+ versus Rb^+), as the slope of the titration curves for the adsorption of Sr^{2+} in both NaCl and RbCl media were the same (Fig. 3a). Conversely, the electrolyte cation did impact the development of surface charge at high ionic strength, 0.3 m (Fig. 3b). The distinct response of Sr^{2+} adsorption to the type of electrolyte ion (Rb^+ or Na^+) at high versus low ionic strength may be due to direct competition of electrolyte cations for inner-sphere binding sites.

The effects of ionic strength on Ca^{2+} and Sr^{2+} adsorption are further evident in Fig. 4. Clearly, in NaCl media the titration curves for the adsorption of both Ca^{2+} and Sr^{2+} are equivalent at 0.03 and 0.3 m ionic strength (Fig. 4a and b). However, in RbCl media (Fig. 4c) the titration curve for Sr^{2+} adsorption in 0.03 m is enhanced slightly relative to the 0.3 m ionic strength data. These differences in the titration curves for the adsorption of Sr^{2+} in NaCl versus RbCl media at 0.3 m ionic strength are consistent with the differences observed in the net proton adsorption electrolyte titration curves, at high pH and 0.3 m ionic strength (Fig. 2b).

Adsorption 'pH edge' data for Sr^{2+} are presented in Fig. 5. A slight ionic strength effect is apparent (Fig. 5), as the adsorption edges are at slightly higher pH values at 0.3 m relative to 0.03 m ionic strength. The type of ionic media has little effect on the 'pH edge' data. The slight ionic strength effects observed for Ca^{2+} and Sr^{2+} are consistent with inner-sphere adsorption onto the rutile surface. Furthermore, the differences in Sr^{2+} adsorption in NaCl versus RbCl media at 0.3 m ionic strength are most likely the result of less effective competition by the larger Rb^+ electrolyte cation than the smaller Na^+ ion.

4. SURFACE COMPLEXATION MODELING

4.1. MUSIC model

The essence of the MUSIC model framework is a thermodynamic model that is based as closely as possible on molecular-level insights. The MUSIC model recognizes and utilizes the specific crystal structure and bonding geometries of the surface functional groups (≡S—OH) of the mineral of interest. As discussed above, the proton affinity constants (pK_a values) are estimated using a simple relationship that correlates the formal charge of the surface groups with thermodynamic constants, as determined for

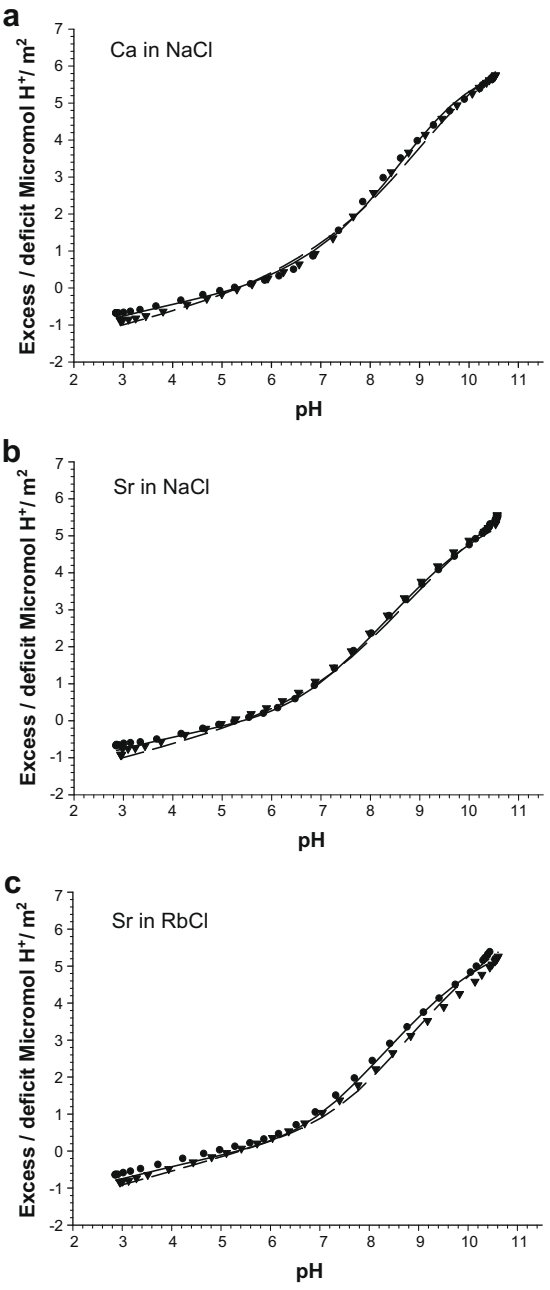

Fig. 4. CD–MUSIC model fits of the relative proton adsorption/desorption and pH titration data for the adsorption of Ca^{2+} and Sr^{2+} at the rutile surface. All model parameter values are defined in the text and given in Table 1. The symbols represent experimental data at ionic strengths of 0.03 (●) or 0.3 m (▼). The best-fit model curves are shown at 0.03 (solid lines) and 0.3 m (dashed lines).

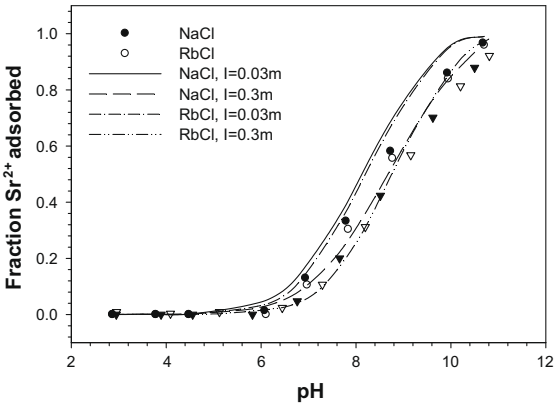

Fig. 5. Adsorption "pH edge" data for the fraction of Sr^{2+} adsorbed to the rutile surface relative to total available Sr^{2+} in the system, as a function of pH. The symbols represent experimental data at ionic strengths of 0.03 (circles) or 0.3 m (triangles), in NaCl (closed symbols) and RbCl (open symbols) media. All curves represent the CD–MUSIC model best-fits. All model parameter values are defined in the text and are given in Table 1.

solution complexes (Hiemstra et al., 1996). Moreover, the refined MUSIC model permits estimation of highly relevant proton affinity constants that incorporate surface relaxation and detailed information on the number and strength of hydrogen bond lengths, as determined from theoretical calculations. The most recent application of the MUSIC model to rutile is due to Machesky et al. (2008), but previous descriptions also exist (Hiemstra et al., 1996; Machesky et al., 2001; Ridley et al., 2002, 2004, 2005; Zhang et al., 2004; Van Riemsdijk and Hiemstra, 2006).

The predominant crystallographic face of the Tioxide powdered rutile used is the (1 1 0) plane (Machesky et al., 2006, 2008; Ridley et al., 2002). Moreover, this correlates with the suggestion of Jones and Hockey (1971) that the (1 1 0), (1 0 0) and (1 0 1) faces predominate on rutile powders, in a ratio of ~0.6:0.2:0.2. For this representation of rutile surfaces two independent reactive surface groups are present: singly coordinated (or terminal, ≡Ti─OH) hydroxyls and double coordinated (or bridged, $\equiv Ti_2O$) surface oxygen atoms, in an ideal 1:1 ratio. The total surface site density, N_S, dictated by crystallographic constraints, and used in all modeling efforts, was taken to be 12.5 sites/nm^2 (20.8 μmol/m^2) (Jones and Hockey, 1971). The protonation reactions, protonation constants, fractional charges and experimental pH_{znpc} values of the rutile used in this study have been discussed in great detail by Machesky et al. (2001, 2006) and Ridley et al. (2002, 2005). In the present communication, all MUSIC model surface protonation constants are taken from Machesky et al. (2008), and are represented by:

$$\equiv TiOH^{-0.434} + H^+ \Longleftrightarrow \equiv TiOH_2^{+0.566} \quad K_{H1} \tag{1}$$

$$\equiv Ti_2O^{-0.555} + H^+ \Longleftrightarrow \equiv Ti_2OH^{+0.445} \quad K_{H2} \tag{2}$$

The log K_{H1} and log K_{H2} values are equal to 5.94 and 4.89 at 25 °C, respectively leading to a corresponding pH_{znpc} of 5.4. This predicted pH_{znpc} precisely matches that observed experimentally, and as detailed in Machesky et al. (2008) this exact match was obtained by slight, arbitrary adjustments (<0.05 Å) to interfacial Ti─O bond lengths as obtained from recent static density functional theory calculations (Bandura et al., 2008). In any case, a precise match between predicted and experimental pH_{znpc} values permits the underlying surface protonation constants (and associated fractional charges) to be held strictly constant for the surface complexation modeling results presented here.

4.2. Electric double layer description

An optimal Surface Complexation Model (SCM) allows for a realistic description of the macroscopic ion adsorption data while also incorporating molecular-level detail. Moreover, a complete SCM comprises adsorption constants for ion binding to the surface functional groups and incorporates a description of the EDL. An appropriate description of the EDL is essential to account for the charge development at the interface, arising from ion adsorption processes. The most commonly utilized EDL model is a Stern-based approach that combines one or more Helmholtz or Stern planes and a diffuse layer (Westall and Hohl, 1980).

The location of the charge of electrolyte ions plays a dominant role in the charge development of surfaces. It has typically been assumed that most electrolyte counterions and co-ions form outer-sphere complexes (i.e. non-specific adsorption). In the simplest approach, the finite size of hydrated counterions imparts a minimum distance of approach of the ions to the surface; therefore, outer-sphere electrolyte ions will be located at a distinct distance to the surface within the EDL (Hiemstra and Van Riemsdijk, 2006). The specific adsorption of ions results in penetration of the compact part of the double layer, thereby forming inner-sphere complexes that have one or more ligands in common with the surface. In the case of rutile, it has been demonstrated conclusively that single-crystal rutile (1 1 0) surfaces specifically adsorb Rb^+ ions at high pH and ionic strength (Zhang et al., 2004, 2007). No evidence for specific adsorption of anions on the rutile surface has been identified in X-ray standing wave studies, although such studies can only probe the interaction of Br^- ions and not Cl^- ions (Zhang et al., 2004). Similarly, MD simulations by Předota et al. (2004b) demonstrated very low affinity of the rutile surface for Cl^- ions, at least to the lower pH limit readily accessible to titration (~2.5). Therefore, it may be reasonably assumed that Cl^- ions form outer-sphere complexes and will not approach the rutile surface as closely as mono- and divalent cations. Consequently, Cl^- will determine the outer limits of the Stern layer or the head of the diffuse double layer. Differences in the reactivity of cations and anions are responsible for the asymmetric charging titration curves for electrolyte ions (Fig. 1), and demonstrate the stronger affinity for cations than anions (as discussed above).

X-ray standing wave measurements show that Sr^{2+} and Rb^+ specifically adsorb to the (1 1 0) rutile surface at high pH; moreover, both ions adsorb in tetradentate geometry (Zhang et al., 2004). This tetradentate geometry comprises two terminal ($\equiv$Ti—OH) and two bridged ($\equiv Ti_2O$) surface sites. Recent MD simulations by Předota and Vlček (2007b) confirm the tetradentate adsorption geometry for Rb^+, Sr^{2+}, Na^+ and Ca^{2+}, although for Na^+ and Ca^{2+} bidentate adsorption geometries appear to predominate. By inference, it may be assumed that K^+ also adsorbs to the rutile surface in tetradentate fashion. Regardless, Zhang et al. (2004) show that at high pH there is a strong positive correlation between the bonding distance of specifically adsorbed cations to the rutile (1 1 0) surface and the bare cation radius. Therefore, within the EDL each ion will be accommodated at some discrete distance from the rutile surface, dependent primarily on the ion size and adsorption geometry.

4.3. The charge distribution (CD) model

The fitting of electrolyte and trace ion adsorption data of a complex multi-component system would be cumbersome and impractical if an individual electrostatic plane was considered for each adsorbing ion. The number of capacitance values and binding constants required to fit a multi-component system would result in considerable covariance, be poorly constrained, and would most likely not result in statistically better fits. Furthermore, the fitting parameters would vary for each system considered as a function of solution composition. The approach in which ions are treated as a single point charge becomes problematic for elements that have hydroxyls and/or oxygen ions in their primary coordination sphere. The charge of the central ion (e.g., Al^{3+}, Si^{4+}, P^{5+}, S^{6+} etc.) and the ligands (OH^-, O^{2-}) have to be located within the EDL. The charge of the ligands is either at the surface or is present outside the surface in the compact part of the double layer. These practical and theoretical difficulties can be circumvented by utilizing the CD approach. In the CD model two electrostatic planes are considered to represent the electrostatic position of an inner-sphere complex. Conversely, in a single point charge approach each adsorbing species requires an individual electrostatic plane characterized by a capacitance. From a practical perspective, the use of only two electrostatic planes is welcomed, reducing the number of parameters that are difficult to constrain.

The CD value may be linked to the structure of the inner-sphere surface complexes. In the simplest approach, the interfacial CD value is determined by the distribution of the ligands in the compact part of the double layer, assuming an equal distribution of charge within the coordination sphere, i.e. a Pauling bond valence charge distribution (Hiemstra and Van Riemsdijk, 1996). In the case of adsorbed cations, the primary hydration shell of each cation may be used as a measure for the total number of ligands in the coordination sphere of the inner-sphere complex. When cations adsorb as inner-sphere surfaces species common ligands form between the cations and the metal-oxide surface, resulting in the release of some primary hydration waters. The corresponding bond valence charge will now be used for the neutralization of the surface ligands that are part of the newly formed complex. This will increase the overall surface charge and in this way it will affect the protonation of surface ligands in general, resulting in an experimentally accessible proton release, known as the proton-ion exchange ratio. It has been shown that this ratio can be linked thermodynamically to the pH dependence of ion binding. In other words, the surface charge attribution is an essential factor for the pH dependency of ion adsorption. The above picture also shows that the surface charge attribution is related to the structure of the adsorbed species. The relative amount of ligands in the coordination sphere of the ion that is common with the surface will play

an important role based on the above sketched bond valence approach (Rietra et al., 1999). It illustrates how charge distribution and the structure of surface complexes can be linked. Spectroscopic information provides molecular-level detail on the structure of inner-sphere adsorbed ions. The actual CD values may be estimated by calculation combining spectroscopic information on the surface coordination, with information on the primary hydration shell of the adsorbed ion, but may also be fitted from proton-ion exchange ratios (Rietra et al., 1999). The use of calculated CD values will have the advantage that the number of fitted parameters will be further reduced and in consequence will better constrain values for the binding constants and the Stern layer capacitance.

4.4. Modeling approach

The starting point of the modeling approach used here was a MUSIC model description of the surface site protonation of the rutile surfaces defined by Machesky et al. (2008), and outlined above. These protonation constants (K_{H1} and K_{H2}) and corresponding site densities (N_S) were fixed for further modeling purposes. All monovalent background electrolyte titration data (Figs. 1 and 2) were fitted simultaneously, allowing inner-sphere and outer-sphere complexation. The charge of inner-sphere complexes was distributed between the surface (0-plane) and Stern plane; in addition, outer-sphere species were allowed as point charges located at the Stern plane that also coincides with the head of the diffuse double layer. The possible presence of these species is found by fitting. Fitting parameters included the binding constant for each type of ion and complex (K_{Cn} and K_A), and a common capacitance value for the Stern layer (C_S) was also fitted.

In all modeling, we explicitly have limited the possible mono- and divalent cation inner-sphere complexes to those identified in the X-ray study of Zhang et al. (2004) and MD simulations of Předota and Vlček (2007b), which both concern cation adsorption on the rutile (1 1 0) surface. On this surface there are 6 possible adsorption configurations (Zhang et al., 2007): 2 monodentate (to the terminal and bridged oxygens), 3 bidentate (terminal–terminal, terminal–bridged, bridged–bridged), and tetradentate (to 2 terminal and 2 bridged oxygens). Moreover, given that terminal groups are further above the 1 1 0 surface plane than bridged groups, and that inner-sphere cation binding distances vary both with bare radii and binding configuration (monodentate > bidentate > tetradentate), implies that even for this simple ideal surface, a complete point-charge description of adsorption for a particular ion could theoretically require up to 6 separate Stern layers. This would clearly be untenable within current SCMs, which at best can accommodate no more than 3 separate Stern layers under a point charge approach. A distinct advantage of the CD approach in this regard is that effort is placed on defining an effective "electrostatic distance" at the interface, relative to fewer (one or two) Stern layers.

In a first modeling step of the primary titration data (Figs. 1 and 2), the charge distribution value (CD_n) of each chosen inner-sphere complex was treated as a fitting parameter. In a second step, the modeling was done using CD values that were calculated from a Pauling bond values approach using the available X-ray and MD information on ion adsorption structures (Tables 1 and 2). These calculated CD values were then fixed during subsequent optimization of the binding constants and Stern layer capacitance values. Parameter optimization was done by combining the speciation program ECOSAT (Keizer and Van Riemsdijk, 1998) with a recent version of FIT (Kinniburgh, 1993).

All parameters derived for the monovalent electrolyte ions were held constant when modeling the divalent cation (Ca^{2+} and Sr^{2+}) adsorption data. As for the monovalent electrolyte-only data, all Ca^{2+} and Sr^{2+} adsorption data in both NaCl and RbCl media were fit simultaneously. However, the net proton charge data (Fig. 4) were fit separately from adsorption 'pH edge' data for Sr^{2+} (Fig. 5), in iterative fashion to obtain the best fits. Both inner-sphere and outer-sphere adsorption species were considered for the adsorption of Ca^{2+} and Sr^{2+} to the rutile surface. As for the monovalent cations, the charge of inner-sphere species was distributed between the surface and the Stern plane. Once again, in initial fitting CD was treated as a fitting parameter. Additionally, the available X-ray and MD information was utilized to calculate CD values, and binding constants were optimized with CD fixed at the calculated value (Tables 1 and 2). Consequently, by considering the relationship between the CD value and structure of the adsorbed species, it was possible to minimize the total number of fitting parameters necessary to describe the macroscopic ion adsorption data.

Table 1
CD–MUSIC Basic Stern model constants and variable parameter values for mono- and divalent cation adsorption onto rutile. The fitted Stern layer capacitance value is $C_1 = 0.64 \pm 0.01$ F/m^2. The calculated charge distribution values (Δz_0 and Δz_1) are also listed. The standard deviation is given for all fitted parameter values.

Ions	log K	Δz_0	Δz_1
Surface protonation			
$\equiv TiOH_2^{+0.566}$	5.94[a]	1	0
$\equiv Ti_2OH^{+0.445}$	4.89[a]	1	0
Inner-sphere complexes			
$(\equiv TiOH^{-0.434})_2(\equiv Ti_2O^{-0.555})_2{-}Na^+$	-1.03 ± 0.020	0.67	0.33
$(\equiv TiOH^{-0.434})_2{-}Na^+$	0.29 ± 0.023	0.33	0.67
$(\equiv TiOH^{-0.434})_2(\equiv Ti_2O^{-0.555})_2{-}K^+$	0.084 ± 0.017	0.50	0.50
$(\equiv TiOH^{-0.434})_2(\equiv Ti_2O^{-0.555})_2{-}Rb^+$	-0.054 ± 0.024	0.50	0.50
$(\equiv TiOH^{-0.434})_2(\equiv Ti_2O^{-0.555})_2{-}Ca^{2+}$	0.58 ± 0.036	1.33	0.67
$(\equiv TiOH^{-0.434})(\equiv Ti_2O^{-0.555}){-}Ca^{2+}$	1.58 ± 0.079	0.67	1.33
$(\equiv TiOH^{-0.434})_2(\equiv Ti_2O^{-0.555})_2{-}Sr^{2+}$	1.20 ± 0.080	1.14	0.86
$(\equiv TiOH^{-0.434})(\equiv Ti_2O^{-0.555}){-}Sr^{2+}$	1.08 ± 0.60	0.57	1.43
Outer-sphere species			
$(\equiv TiOH^{-0.434})_2{-}K^+$	0.51 ± 0.12	0	1
$(\equiv TiOH^{-0.434})_2{-}Rb$	1.08 ± 0.077	0	1
$(TiOH_2^{+0.566}){-}A^-$ and $(\equiv Ti_2OH^{+0.445}){-}A^-$	0.10 ± 0.06	0	−1

[a] From Machesky et al. (2008).

Table 2
Fitted versus calculated CD values, with the calculated values based on Pauling bond valence principles.

Ions	Fitted Δz_0	CN	Calculated Δz_0
$(\equiv TiOH^{-0.434})_2(\equiv Ti_2O^{-0.555})_2{-}Na^+$	0.77 ± 0.088	6	0.67
$(\equiv TiOH^{-0.434})_2{-}Na^+$	0.39 ± 0.017	6	0.33
$(\equiv TiOH^{-0.434})_2(\equiv Ti_2O^{-0.555})_2{-}K^+$	0.49 ± 0.010	8	0.50
$(\equiv TiOH^{-0.434})_2(\equiv Ti_2O^{-0.555})_2{-}Rb^+$	0.47 ± 0.013	8	0.50
$(\equiv TiOH^{-0.434})_2(\equiv Ti_2O^{-0.555})_2{-}Ca^{2+}$	1.23 ± 0.024	6	1.33
$(\equiv TiOH^{-0.434})(\equiv Ti_2O^{-0.555}){-}Ca^{2+}$	0.90 ± 0.075	6	0.67
$(\equiv TiOH^{-0.434})_2(\equiv Ti_2O^{-0.555})_2{-}Sr^{2+}$	1.18 ± 0.021	7 (6–8)	1.14
$(\equiv TiOH^{-0.434})(\equiv Ti_2O^{-0.555}){-}Sr^{2+}$	0.65 ± 0.051	7 (6–8)	0.57

5. MODELING RESULTS AND DISCUSSION

5.1. Monovalent electrolyte ion adsorption

The best-fit model curves for the titration data of rutile in monovalent electrolyte media are shown in Figs. 1 and 2, and the associated values of the variable fitting parameters are presented in Table 1. For each electrolyte, the fits include an inner-sphere tetradentate species for cations, as identified by X-ray spectroscopy and MD simulations (Zhang et al., 2004), which is represented by,

$$2(\equiv TiOH^{-0.434}) + 2(\equiv Ti_2O^{-0.555}) + C^+ \Longleftrightarrow [(\equiv TiOH^{-0.434})_2(\equiv Ti_2O^{-0.555})_2]^{\Delta z0} - C^{\Delta z1} \quad K_{C\text{-tet}} \qquad (3)$$

The charge of these inner-sphere complexes was distributed over the surface (0-plane) and Stern planes, and was expressed as Δz_0 and Δz_1, respectively ($\Delta z_0 + \Delta z_1 = 1$). The quality of the fits can be markedly improved by considering for the various cations an additional surface adsorption species. The nature of this species is different for the different ions considered, but the various species are consistent with those identified in the recent MD simulation results of Předota and Vlček (2007b). In addition to the tetradenate species, Předota and Vlček (2007b)) identified two of the three possible bidenate adsorption geometries at the effective $-0.2\ C/m^2$ surface charge of their simulations (equivalent to approximately $+2$ μmols H^+ in Figs. 1–4) as being present (terminal–terminal, and terminal–bridged). For Na^+ the terminal–terminal surface species predominates (52%), followed by the tetradentate species (28%). In contrast, the terminal–bridged Na^+ complex comprised a smaller fraction of the adsorbed Na^+ ions (16% occupancy). Ultimately, only the terminal–terminal bidenate and tetradentate species were considered for the final fitting of the NaCl electrolyte data (Fig. 1). Inclusion of the terminal–bridged bidentate complex did not improve the quality of the fit; moreover, three binding constants resulted in considerably more covariance among the parameters. The two Na^+ adsorption configurations (i.e., tetradentate and terminal–terminal bidentate species) were considered as inner-sphere species, and occur at heights less than 3.8 Å above the rutile (1 1 0) surface (Předota and Vlček, 2007b). Předota et al. (2004b) defined all adsorbed ion heights relative to a plane bisecting the centers of surface Ti and O atoms on the rutile (1 1 0) surface that has ideal bulk structure. The inner-sphere terminal–terminal bidentate species is represented by,

$$2(\equiv TiOH^{-0.434}) + Na^+ \Longleftrightarrow (\equiv TiOH^{-0.434})_2^{\Delta z0} - Na^{\Delta z1} \quad K_{Na\text{-bid}} \qquad (4)$$

For Rb^+ ions, the MD simulation results of Předota and Vlček (2007b) indicated that the tetradenate species predominates (79% occupancy), with the small remaining occupancy distributed equally between the terminal–terminal and terminal–bridged bidenate complexes. As the fraction of each Rb-bidentate species was small (<20% occupancy, (Předota and Vlček, 2007b)), these were combined into a single terminal–terminal bidenate species for the present SCM efforts. From the MD simulation results (Předota and Vlček, 2007b), the binding heights for the Rb-tetradentate species was less than 3.8 Å above the rutile (1 1 0) surface; whereas, the Rb-bidentate species were at heights greater than 4.2 Å. The charge of the Rb-bidenate species was fully attributed to the Stern plane, comparable to an outer-sphere point charge complex ($\Delta z_0 = 0$ and $\Delta z_1 = 1$).

For the K^+ ion, the titration data were fitted using the same binding configurations as for Rb^+, given that the bare cation radii are similar (Rb^+ 1.49 Å and K^+ 1.38 Å; (Marcus, 1997)). These terminal–terminal bidenate species for Rb^+ and K^+ are represented by,

$$2(\equiv TiOH^{-0.434}) + C^+ \Longleftrightarrow (\equiv TiOH^{-0.434})_2 - C^+ \quad K_{C\text{-bid}} \qquad (5)$$

As summarized above, available X-ray and MD simulation results suggest only weak interaction of Cl^- with the rutile surface, at least within the pH and charge range accessible by our titrations ($pH > 2.5$ and charge > -1 μmols H^+/m^2, e.g., Fig. 1). Therefore, the modeling strategy for Cl^- was simple and rather conventional. That is, monodentate, outer-sphere point charge binding to the terminal and bridged groups, with the binding constants constrained to be equal for both. The two Cl^- species are represented by,

$$\equiv TiOH_2^{+0.566} + A^- \Longleftrightarrow (\equiv TiOH_2^{+0.566}) - A^- \quad K_{A1} \qquad (6)$$

$$\equiv Ti_2OH^{+0.445} + A^- \Longleftrightarrow (\equiv Ti_2OH^{+0.445}) - A^- \quad K_{A2}. \qquad (7)$$

5.2. Divalent cation adsorption

Both the X-ray spectroscopic results of Zhang et al. (2004), and the MD results of Předota and Vlček (2007b) unequivocally identify a dominant tetradentate binding

geometry for Sr^{2+}. Additionally, both terminal–terminal and terminal–bridged bidentate complexes were identified from the MD simulations, with the terminal–bridged configuration predominating (20% versus 10% coverage). For the smaller Ca^{2+} cation, the MD simulation results of Předota and Vlček (2007b) suggest a more equal distribution between the tetradentate (31%), terminal–bridged (34%), and terminal–terminal configurations (22%) at -0.2 C/m^2 surface charge. Consequently, for the purposes of simplification, only the more dominant tetradentate and terminal–bridged species were considered when fitting the titration data for both Sr^{2+} and Ca^{2+}. These two inner-sphere complexes are represented by,

$$2(\equiv TiOH^{-0.434}) + 2(\equiv Ti_2O^{-0.555}) + M^{2+} \Longleftrightarrow [(\equiv TiOH^{-0.434})_2(\equiv Ti_2O^{-0.555})_2]^{\Delta z0} - M^{\Delta z1} \quad K_{M\text{-}tet} \qquad (8)$$

and

$$(\equiv TiOH^{-0.434}) + (\equiv Ti_2O^{-0.555}) + M^{2+} \Longleftrightarrow [(\equiv TiOH^{-0.434})(\equiv Ti_2O^{-0.555})]^{\Delta z0} - M^{\Delta z1} \quad K_{M\text{-}bid} \qquad (9)$$

As with the inner-sphere complexes for the monovalent electrolyte ions, the charge of Ca^{2+} and Sr^{2+} was distributed over the surface and Stern planes (i.e., expressed as Δz_0 and Δz_1, respectively, with $\Delta z_0 + \Delta z_1 = 2$).

The tetradentate binding constants for Ca^{2+} and Sr^{2+} (Table 1) are considerably larger than the corresponding binding constants for the monovalent cations, which reflects the observed enhanced proton desorption (Fig. 3). For Sr^{2+} adsorption edge data were also available. Accordingly, both sets of Sr^{2+} data were fit iteratively with the tetradentate and bidentate binding constants as the only variable parameters. Although the resulting fits to the Sr^{2+} proton desorption data (μmols H^+/m^2) were excellent (Figs. 3 and 4), the fits to the more limited adsorption pH edge data were not as good, with predicted adsorption overestimating that measured (Fig. 5).

5.3. Charge distribution values

As outlined above, preliminary modeling allowed for fully free optimization of the CD values and binding constants. The freely-fitted CD values for all inner-sphere species are presented in Table 2 along with the calculated (predicted) CD values. In calculating CD values it was assumed that formation of a common ligand upon adsorption of a cation leads to the release of one hydration water from the primary hydration shell of the cation. In addition, an equal distribution of charge within the primary hydration sphere of the adsorbing cations was assumed, i.e. a Pauling bond valence distribution. Moreover, MD simulations suggest that these inner-spherically adsorbed cations remain partially hydrated (Předota et al., 2004a; Předota et al., 2007a). The reported number of H_2O molecules in the primary hydration shell of the electrolyte ions (i.e., Na^+, K^+, and Rb^+) are somewhat variable and depend on method, with values between 5 and 8 being most frequently cited (Marcus, 1988; Richens, 1997; Ikeda et al., 2007). Primary hydration numbers generally increase with cation size. The primary hydration numbers used to estimate CD values are listed in Table 2.

When cations adsorb as tetradentate surface species four primary hydration waters are estimated to be released from the absorbing cation. In the case of an overall coordination number of 6 or 8, the expected CD value for the formation of an inner-sphere tetradentate adsorption of monovalent cations will be, respectively, $\Delta z_0 = 0.67$ and $\Delta z_0 = 0.50$ v.u. Likewise, inner-sphere bidentate adsorption would release two primary hydration sphere water molecules. The bidentate adsorption of ions with CN = 6 or 8 would result in Δz_0 values half as large. Reported values for the primary hydration sphere of Ca^{2+} are somewhat variable (6–9), although recent computational studies suggest 6–7 water molecules are slightly preferred (Naor et al., 2003; Ikeda et al., 2007). Primary hydration numbers between 6 and 8 are reported for Sr^{2+}, with 8 being the most often reported value (Richens, 1997; Seward et al., 1999; Harris et al., 2003). With a primary hydration coordination number of 6, the calculated CD values for tetradentate and bidentate adsorption geometries of divalent cations are $\Delta z_0 = 1.33$ and 0.67 v.u., respectively. Similarly, the calculated CD values for divalent cations with 7-fold coordination are $\Delta z_0 = 1.14$ and 0.57 v.u. for tetradentate and bidentate surface complexes, respectively.

During initial fitting with free optimization of CD, the best fit CD values for K^+ and Rb^+ adsorbed in tetradentate coordination were 0.49 (±0.010) and 0.47 (±0.013), respectively. These values are very close to the calculated CD value of 0.5 expected for a primary hydration number of 8. Correspondingly, best-fit CD values for Na^+ were near the calculated values of 0.67 for tetradentate and 0.33 for bidentate binding (0.77 ± 0.088 and 0.39 ± 0.017 for tetradentate and bidentate binding, respectively), as expected for a primary hydration number near 6 (Table 2). The best-fit CD value for the Sr^{2+} surface charge (proton desorption) data was 1.18 (±0.021); close to that predicted for a primary hydration number of 7 ($\Delta z_0 = 1.14$ v.u.). A value which is within the reported range of 6–8 (Richens, 1997; Seward et al., 1999; Harris et al., 2003). For the more limited Sr^{2+} adsorption edge data (Fig. 5), the best fit CD value tended towards values somewhat less than 1.14 (~1). Conversely, the best-fit CD value for the bidentate Sr^{2+} surface species was 0.65 (±0.051), which is very close to the calculated CD value of 0.67 for 6-fold coordination. The predicted CD values for a hydration number of 7 were therefore used as a reasonable average for the final fitting of the Sr^{2+} data. The freely optimized CD value of 1.23 (±0.024) for the adsorption of Ca^{2+} in tetradentate coordination is comparable to the calculated CD value of 1.33 for a primary hydration number of 6. Somewhat poorer agreement between the best-fit (0.90 ± 0.075) and calculated CD (0.67) values was observed for the Ca-bidentate species. The slightly higher fitted CD values, compared to the calculated values, for the smaller Ca^{2+} and Na^+ ions suggests that these ions lie closer to the rutile surface than the larger cations; agreeing with both X-ray (Zhang et al., 2004) and MD simulations (Předota and Vlček, 2007b).

Taken as a whole, the fitted CD values agree rather well with those predicted from assuming that the cations adsorb inner-spherically, predominantly in tetradentate and bidentate geometry, and retain their remaining primary hydra-

tion waters. This is especially pertinent given the relatively simple Basic Stern layer description of the EDL used, and the all-inclusive modeling framework employed here. And certainly, even better agreement between fitted and calculated CD values would be possible by including an additional layer within the EDL (i.e., a three layer model), thus accounting for the closer approach of the smaller Ca^{2+} and Na^{+} ions to the rutile surface. Moreover, estimation of the CD values could be refined further by considering the relative bond lengths in the coordination shell in combination with a correction for changes in water dipole orientation (Hiemstra and Van Riemsdijk, 2006).

Allowing for fully free optimization of the CD values results in a considerable number of fitting parameters; moreover, there was a great degree of covariance between those fitted parameters. Particularly, the CD values and binding constants values are highly negatively correlated. Linear correlation coefficients between the binding constant for the tetradentate species and corresponding CD values were less than −0.87; whereas, the correlation coefficients between CD and the bidentate binding constants was less than −0.60. Furthermore, the bidentate and tetradentate binding constants and CD values were also correlated among themselves. For example, the correlation coefficient between the tetradentate and bidentate binding constants for Ca^{2+} was −0.71. In comparison, when the CD value was a fixed parameter (i.e. parameters reported in Table 1) the correlation coefficients between the tetradentate and bidentate binding constants were typically lower, ranging from −0.64 to 0.45. Nevertheless, the resulting fit was nearly identical, due in part to the relatively high degree of correlation between binding constants and CD values.

5.4. Surface speciation

Representative surface site speciation diagrams calculated with the parameter values in Table 1 for electrolyte media only and with Ca^{2+} or Sr^{2+} present, are presented in Figs. 6 and 7, respectively. For clarity, only the surface species with adsorbed cations are shown. The predominant uncomplexed positive surface site was $\equiv TiOH_2^{+0.566}$, whereas $Ti_2O^{-0.555}$ was the dominant bare negative surface site over the entire 3–10.5 pH titration range. This reflects that the bridged group is more acidic than the terminal group according to the MUSIC model, and IR spectroscopy results independently support this contention (Connor et al., 1999). Uncomplexed $Ti_2O^{-0.555}$ sites decreased in abundance as pH increased primarily due to tetradentate and/or bidentate cation binding. The binding of Cl^{-} was minor (<10% coverage) over the entire titration pH range.

Changes in surface speciation as a function of pH and ionic strength can be understood based on the location of the charge of the different species at the interface. The most noticeable feature in both Figs. 6 and 7 is the significant fraction of the surface sites associated with the tetradentate species as pH increases above the pH_{znpc}. For Na^{+}, the bidentate species predominates over the tetradentate species at pH values below 10, in agreement with the MD simulation results of Předota and Vlček (2007a). The MD simulation results (Předota and Vlček, 2007a) indicated that the bidentate:tetradentate complex ratio was approximately 2 at a surface charge of $-0.2\ C/m^2$, which occurs at around pH 9 (Fig. 1). Furthermore, at high ionic strength (0.3 m) some Na^{+} is adsorbed in bidentate coordination below the pH_{znpc}, indicative of strong intrinsic affinity between the surface sites and the Na^{+} ions. The abundance of the Rb-tetradentate surface species is lower at all pH conditions than the corresponding K^{+} tetradentate species (Fig. 6), reflecting the intrinsic lower affinity for Rb^{+} (Table 1). Additionally, the outer-sphere Rb complex is rather abundant, reflecting the relatively large log K value fit for this species (1.08).

In a recent study, Zhang et al. (2007) investigated the structure of the rutile (1 1 0)-aqueous solution interface in 1 molal RbCl solution at pH 12 with the X-ray crystal truncation rod method. The tetradentate adsorption structure for Rb^{+} was observed; in addition, the surface coverage of this species was estimated to be 0.4 (±0.1) monolayer (1 monolayer = 1 Rb^{+} per 19.24 Å^2) (Zhang et al., 2007). Using the CD–MUSIC model parameters for Rb^{+} given

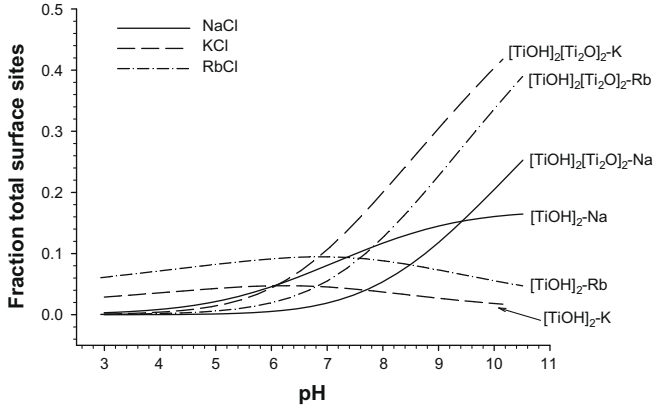

Fig. 6. The distribution of surface species on rutile in solutions comprising electrolyte only at $I = 0.3$ m. The plots show inner- and outer-sphere electrolyte cation surface species, presented as fractions of the total concentration of surface sites, N_S, which was fixed at 20.8 μmol/m^2. The anion surface species are omitted for clarity; however, except at low pH conditions the total fraction of anion surface-species is always small.

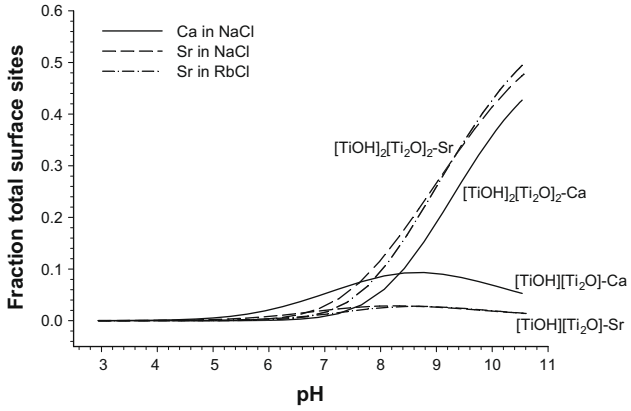

Fig. 7. The distribution of surface species on rutile in solutions at $I = 0.3$ m in NaCl or RbCl media, with 0.001 m initial Ca^{2+} or Sr^{2+}. The plots show the divalent cation adsorption species, presented as fractions of the total concentration of surface sites, N_S, which was fixed at 20.8 μmol/m^2. The electrolyte surface species are omitted for clarity; however, the total fraction of the electrolyte surface-species was generally small and always less than 15% of the available surface sties.

in Table 1 and extrapolating to solution conditions of 1 molal and pH 12 results in a predicted coverage of about 0.35 monolayer. Despite extrapolating beyond the experimental conditions, the calculated coverage is in good agreement with the value estimated by Zhang et al. (2007). Moreover, this agreement is significantly better than the coverage estimated from extrapolation of model results that considered Rb^+ to be a simple point charge (~0.2 monolayer).

For clarity, only the divalent surface species have been shown in Fig. 7, however, it is apparent that adsorption of the divalent species suppresses Na^+ and Rb^+ counterion binding, due principally to the higher divalent charge. In fact, over the entire pH range, less than 15% of the total surface sites are covered by monovalent electrolyte ions (including all inner and outer-sphere species) in the presence of Ca^{2+} or Sr^{2+}. Moreover, given a total surface site concentration of 20.8 μmol/m^2, and bidentate and tetradentate coordination, maximum Sr^{2+} or Ca^{2+} surface coverage is ~50% of the available sites for our experimental conditions.

5.5. Electric double layer structure

Our understanding of the solid–solution interfacial region has advanced significantly through the incorporation of molecular-level detail into SCMs (for example, (Venema et al., 1996b; Rietra et al., 2001; Zhang et al., 2004; Boily et al., 2005). However, these models are still unable to provide detailed structural information about the EDL by themselves. The approach taken here was aimed towards better characterizing the EDL of a multi-component system: a Basic Stern layer description of the EDL was found to be the most suitable for this purpose. Recently, it has been suggested that due to structuring of water near the surface, charge separation may exist between the head end of the diffuse double layer and the Stern plane (Hiemstra and Van Riemsdijk, 2006). For goethite, the Basic Stern model was extended with a second Stern layer to account for this. In this study, such an extension was found to be unnecessary for the rutile–water interface, and there may be two possible reasons for this. First, water molecules may be structured significantly differently at the rutile and goethite interfaces. Although, molecular-scale information concerning water structure at the goethite surface is lacking, a recent quasielastic neutron scattering study (Mamontov et al., 2007) demonstrated that water structure and dynamics are distinctly different between rutile and cassiterite (SnO_2) surfaces. In general, water molecules were found to be more tightly bound at the cassiterite surface, which coincidently has a low bulk dielectric constant similar to that of goethite. Second, the dominance of the inner-sphere complexes may also obscure the unveiling of double layer details at larger distances, due to the large charge neutralization in the inner Stern layer and therefore lower potentials at the head end of the DDL (Hiemstra and Van Riemsdijk, 2006).

The modeling results presented here (Table 1) are considerably different from those determined in our earlier modeling efforts which considered all ions to be point charges (Machesky et al., 2001, 2006; Ridley et al., 2004, 2005; Zhang et al., 2004). In particular, the Stern layer capacitance value is much smaller (0.6 vs. ~2), and the Cl^- binding constant much larger (log K_A 0.10 versus <-2). In our previous modeling efforts, best-fit capacitance values depended critically on the electrolyte cation considered, and the electrolyte anion was effectively ignored. In this analysis, however, a single Stern layer capacitance value suffices for all adsorbed species, this capacitance value is constrained by presumed outer-sphere complexation, and charge distribution is used to define the relative electrostatic position of inner-sphere adsorption complexes.

The capacitance of the Stern layer is taken as a general characteristic of the interface region determined by the average minimum distance of approach of all outer-sphere complexes. The Stern layer capacitance is related to the charge separation and the dielectric constant of the Stern layer (ε_S) according to,

$$C_s = \varepsilon_0 \varepsilon_s / d \tag{10}$$

where C_S is the Stern layer capacitance in units of F/m^2, and ε_0 is the permittivity of vacuum (8.854×10^{-12}). The

d term is the distance of charge separation (in meters), and here corresponds to the average distance of the Stern plane from the rutile surface (Hiemstra and Van Riemsdijk, 1991; Stumm, 1992). If measured adsorption distances are available, then the Stern layer dielectric constant (ε_S) would be a unique parameter for a given C_S value. Such descriptions of EDL structure necessitate that the dielectric constant be applied at the microscale, although it is strictly a macroscopic quantity. In addition, in this approach ε_S is assumed to be constant, although it may depend on the (variable) field strength (Hiemstra and Van Riemsdijk, 1991, 2006). The concern of miss-representing the dielectric constant is minimized with a Basic Stern layer description of the EDL, although such a description may oversimplify the EDL structure. Nevertheless, by keeping these various limitations in mind, new insights concerning ion adsorption and the interface region can be obtained when relating the capacitance value, dielectric constant and charge separation.

Using the above expression (Eq. (10)), some interpretations of the Stern layer dielectric constant and/or distance are possible. Unfortunately, no definitive spectroscopic data (for example, EXAFS or X-ray standing wave measurements) are available to precisely pin down actual outer-sphere complexation distances; consequently only potential scenarios can be presented. A maximum Stern layer thickness can be obtained using the best-fit C_S value (0.64 F/m^2) along with the bulk dielectric constant of water ($\varepsilon_b = 78$ at 25 °C) as an estimate for the Stern layer dielectric constant (ε_S). The resulting value for d is 10.8 Å, which equates approximately to the diameter of a Cl^- ion (3.6 Å) and 3 water molecules (2.8 Å each). This seems too large, given that the diameter of the hydrated ions used in this study are closer to 4–5 Å. It is more likely that ε_S is lower than for the bulk solution (ε_b), which is reasonable owing to the high concentration of ions present in the Stern layer region. Additionally, ε_S being less than ε_b would suggest that the near-surface water is somewhat polarized as expected for a charged interface. A more reasonable ε_S estimate is derived by assuming the Stern plane is defined by the average distance of approach of hydrated counter ions (≈bare radii + 2.8 Å). Using $d = 4.3 \pm 0.3$ Å (radius of Rb^+), the resulting value for ε_S is 31 ± 3 at 25 °C, which is considerably lower than ε_b. This value is between the values for bulk water (78) and water at electrostatic saturation (6). Values of ε_S lower than those of bulk water are reasonable for water in a charged field with a potential fall of 100–200 mV within the Stern layer (Hiemstra and Van Riemsdijk, 2006).

6. CONCLUSIONS

This study provides a coherent SCM for electrolyte ion adsorption at mineral surfaces. An extensive suite of potentiometric titration data for electrolyte ions (NaCl, KCl and RbCl) and divalent cation ($CaCl_2$ and $SrCl_2$) adsorption onto the same batch of rutile was simultaneously modeled applying the CD and MUSIC model using a Basic Stern layer description of the EDL. A central theme in this study was to link the macroscopic titration data and available surface structural information, including the specific coordination geometry of inner-sphere species, with the structure of the EDL through application of the CD–MUSIC model. Therefore, the model incorporates relevant information available at the molecular-level. Moreover, to adequately constrain the model and for consistency the MD simulation results of Předota and Vlček (2007a) and X-ray results of Zhang et al. (2004) were utilized.

Explicitly, for all cations the CD–MUSIC model shows that above neutral pH the principal adsorption complex was an inner-sphere tetradentate species, previously identified by X-ray standing wave measurements (Zhang et al., 2004). Besides the tetradentate surface species, bidentate surfaces species were also fitted. For Na^+, the bidentate surface species predominated up to pH values of 9.5, which is in agreement with MD simulation results (Předota and Vlček, 2007a). Outer-sphere bidentate surface species improved the fit of K^+ and Rb^+. As anticipated, the CD model shows that outer-sphere complexation is most significant at pH conditions around the PZC; whereas with increasing pH inner-sphere complexation predominates since the increasingly negative surface potential favors the formation of the inner-sphere complexes for the cations considered.

The difference in pH dependency of the surface speciation can be linked directly to the distribution of charge of cations in the compact part of the interface. Free optimization of the charge distribution was near CD values calculated, based on a Pauling distribution of charge for the coordination geometry of the surface species. Consequently, CD values were set equal to the calculated values for final fitting optimization, thus reducing the total number of fitting parameters. Our modeling shows that the high surface charge found for well-structured rutile can be explained by inner-sphere complexation of electrolyte ions without using an exceptionally high value for the Stern layer capacitance in the modeling.

Collectively, the model results of this work show that application of a relatively simple SCM can incorporate molecular-scale information for a multi-component system, and may provide realistic fitting parameters for complex mineral-aqueous solutions, in particular if the modeling is constrained by the results of X-ray synchrotron measurements and MD simulation results. Moreover, the CD model allows a realistic quantification of surface speciation and is able to explain conditions under which various surface species are dominant.

ACKNOWLEDGEMENTS

This research was supported by the National Science Foundation (EAR-0124001) and by the Office of Basic Energy Sciences, U.S. Department of Energy (contract no. DE-AC05-00OR22725), Oak Ridge National Laboratory, managed by UT-Battelle, LLC. The modeling results presented here were completed while M.K.R. was on sabbatical at Wageningen University, and she thanks Willem van Riemsdijk and Tjisse Hiemstra for hosting her. M.L.M. acknowledges the support of the Illinois State Water Survey and Illinois Department of Natural Resources. We thank Dr Milan Předota from the University of South Bohemia, Czech Republic for his helpful discussions regarding his MD simulations. His input is highly appreciated. The comments and criticisms of Dr

B. Bickmore, two anonymous reviewers, and Associate Editor Dr J. Rustad lead to a much improved final manuscript.

REFERENCES

Axe L., Bunker G. B., Anderson P. R. and Tyson T. A. (1998) An XAFS analysis of strontium at the hydrous ferric oxide surface. *J. Colloid Interf. Sci.* **199**, 44–52.

Bandura A. V., Kubicki J. D. and Sofo J. O. (2008) Comparison of the multilayer adsorption of H_2O on the (110) surfaces of TiO_2 and SnO_2 with the rutile structure. *J. Phys. Chem. B* **112**, 11616–11624.

Berube Y. G. and de Bruyn P. L. (1968) Adsorption at the rutile-solution interface 1. Thermodynamic and experimental study. *J. Colloid. Interf. Sci.* **27**, 305–318.

Boily J.-F., Sjoberg S. and Persson P. (2005) Structures and stabilities of Cd(II) and Cd(II)-phthalate complexes at the goethite/water interface. *Geochim. Cosmochim. Acta* **69**, 3219–3235.

Boily J. F. and Fein J. B. (1996) Experimental study of cadmium-citrate co-absorption onto a-Al_2O_3. *Geochim. Cosmochim. Acta* **60**, 2929–2938.

Boily J. F., Pearson P. and Sjoberg S. (2000) Benzenecarboxylate surface complexation at the goethite (a-FeOOH)/water interface. *J. Colloid Interf. Sci.* **227**, 132–140.

Bourikas K., Hiemstra T. and Van Riemsdijk W. H. (2001) Ion pair formation and primary charging behaviour of titanium oxide (anatase and rutile). *Langmuir* **17**, 749–756.

Brown G. E. and Sturchio N. C. (2002) An overview of synchrotron radiation applications to low temperature geochemistry and environmental science. In *Application of Synchrotron Radiation in Low Temperature Geochemistry and Environmental Science* (eds. P. A. Fenter, M. L. Rivers, N. C. Sturchio and S. R. Sutton). Geological Society of America & Mineralogical Society of America.

Brown G. E. J., Henrich V. E., Casey W. H., Clark D. L., Eggleston C., Felmy A., Goodman D. W., Gratzel M., Maciel G., McCarthy M. I. and Nealson K. H. (1999) Metal oxide surface and their interactions with aqueous solutions and microbial organisms. *Chem. Rev.* **99**, 77–174.

Brown I. D. (2002) The Chemical Bond in Inorganic Chemistry. The Bond Valence Model. Oxford University Press, Oxford.

Brown I. D. and Altermatt D. (1985) Bond-valence parameters obtained from a systematic analysis of the inorganic crystal structure database. *Acta Crystallogr.* **B41**, 244–247.

Connor P. A., Dobson K. D. and McQuillan A. J. (1999) Infrared spectroscopy of the TiO_2 aqueous solution interface. *Langmuir* **15**, 2402–2408.

Davis J. A., James R. O. and Leckie J. O. (1978) Surface ionization and complexation at the oxide/water interface I. Computation of electrical double layer properties in simple electrolytes. *J. Colloid Interf. Sci.* **63**, 480–499.

Davis J. A. and Leckie J. O. (1978) Surface ionization and complexation at the oxide/water interface II. Surface properties of amorphous iron oxyhydroxide and adsorption of metal ions. *J. Colloid Interf. Sci.* **67**, 90–107.

Dzombak D. A. and Morel F. M. M. (1990) Surface Complexation Modeling-Hydrous Ferric Oxide. Wiley.

Fenter P., Cheng L., Rihs S., Machesky M., Bedzyk M. J. and Sturchio N. C. (2000) Electric double-layer structure at the rutile–water interface as observed *in situ* with small-period X-ray standing waves. *J. Colloid Interf. Sci.* **225**, 154–165.

Fenter P. A., Rivers M. L., Sturchio N. C. and Sutton S. R. (2002). *Applications of Synchrotron Radiation in Low-Temperature Geochemistry and Environmental Science*. .

Fitts J. P., Machesky M. L., Wesolowski D. J., Shang X., Kubicki J. D., Flynn G. W., Heinz T. F. and Eisenthal K. B. (2005) Second-harmonic generation and theoretical studies of protonation at the water/α-TiO_2 (1 1 0) interface. *Chem. Phys. Lett.*, 399–403.

Harris D. J., Brodholt J. P. and Sherman D. M. (2003) Hydration of Sr^{2+} in hydrothermal solutions from ab initio molecular dynamics. *J. Phys. Chem. B* **107**, 9056–9058.

Hiemstra T. and Van Riemsdijk W. H. (1991) Physical chemical interpretation of primary charging behaviour of metal (hydr)oxides. *Colloid. Surf.* **59**, 7–25.

Hiemstra T. and Van Riemsdijk W. H. (1996) A surface structural approach to ion adsorption: the charge distribution (CD) model. *J. Colloid Interf. Sci.* **179**, 488–508.

Hiemstra T. and van Riemsdijk W. H. (2006) On the relationship between charge distribution, surface hydration, and the structure of the interface of metal hydroxides. *J. Colloid Interf. Sci.* **301**, 1–18.

Hiemstra T., Van Riemsdijk W. H. and Bolt G. H. (1989) Multisite proton adsorption modeling at the solid/solution interface of (Hydr)oxides: a new approach I. Model description and evaluation of intrinsic reaction constants. *J. Colloid Interf. Sci.* **133**, 91–104.

Hiemstra T., Venema P. and Van Riemsdijk W. H. (1996) Intrinsic proton affinity of reactive surface groups of metal (hydr)oxides: the bond valence principle. *J. Colloid Interf. Sci.* **184**, 680–692.

Ikeda T., Boero M. and Terakura K. (2007) Hydration of alkali ions from first principles molecular dynamics revisited. *J. Chem. Phys.* **126**, 034501–034509.

Jang H. M. and Fuerstenau D. W. (1986) The specific adsorption of alkaline-earth cations at the rutile/water interface. *Colloid. Surf.* **21**, 235–257.

Jones P. and Hockey J. A. (1971) Infra-red studies of rutile surfaces. 2. Hydroxylation, hydration and structure of rutile surfaces. *Trans. Faraday Soc.* **67**, 2679–2685.

Keizer M. G. and Van Riemsdijk W. H. (1998) *ECOSAT. Technical Report Department Soil Science and Plant Nutrition*, Wageningen Agricultural University, Wageningen, The Netherlands.

Kinniburgh D. G. (1993) Fit. *Technical Report WD/93/23, British Geological Survey*, Keyworth, Great Britain.

Machesky M. L., Palmer D. A. and Wesolowski D. J. (1994) Hydrogen ion adsorption at the rutile–water interface to 250 °C. *Geochim. Cosmochim. Acta* **58**, 5627–5632.

Machesky M. L., Předota M., Wesolowski D. J., Vlček L., Cummings P., Rosenqvist J., Ridley M. K., Kubicki J. D., Bandura A., Kumar N. and Sofo J. (2008) Surface protonation at the rutile (110) interface: explicit incorporation of solvation structure within the revised MUSIC model framework. *Langmuir* **24**, 12331–12339.

Machesky M. L., Wesolowski D. J., Palmer D. A. and Ichiro-Hayashi K. (1998) Potentiometric titrations of rutile suspensions to 250 °C. *J. Colloid Interf. Sci.* **200**, 298–309.

Machesky M. L., Wesolowski D. J., Palmer D. A. and Ridley M. K. (2001) On the temperature dependence of intrinsic surface protonation equilibrium constants: an extension of the revised MUSIC model. *J. Colloid Interf. Sci.* **239**, 314–327.

Machesky M. L., Wesolowski D. J., Palmer D. A., Ridley M. K., Bénézeth P., Lvov S. N. and Fedkin M. V. (2006) Ion adsorption into the hydrothermal regime: experimental and modeling approaches. In *Surface Complexation* (ed. J. Luetzenkirchen). Elesevier.

Mamontov E., Vlček L., Wesolowski D. J., Cummings P. T., Wang W., Anovitz L. M., Rosenqvist J., Brown C. M. and GarciaSakai V. (2007) Dynamics and structure of hydration water on rutile and cassiterite nanopowders studied by quasi-

elastic neutron scattering and molecular dynamics simulations. *J. Phys. Chem. C* **111**, 4328–4341.

Marcus Y. (1988) Ionic radii in aqueous solutions. *Chem. Rev.* **88**, 1475–1498.

Marcus Y. (1997) *Ion Properties*. Marcel Dekker, New York, p. 259.

Naor M. M., Nostrand K. V. and Dellago C. (2003) Car-Parrinello molecular dynamics simulation of the calcium ion in liquid water. *Chem. Phys. Lett.* **369**, 159–164.

Parks G. A. and De Bruyn P. L. (1962) The zero point of charge of oxides. *J. Phys. Chem.* **66**, 967–973.

Předota M., Bandura A. V., Cummings P. T., Kubicki J. D., Wesolowski D. J., Chialvo A. A. and Machesky M. L. (2004a) Electric double layer at the rutile (110) surface. 1. Structure of surfaces and interfacial water from molecular dynamics by use of ab initio potentials. *J. Phys. Chem. B* **108**, 12049–12060.

Předota M., Cummings P. T. and Wesolowski D. (2007a) Electric double layer at the rutile (110) Surface. 3. Inhomogeneous viscosity and diffusivity measurement by computer simulations. *J. Phys. Chem. C* **111**, 3071–3079.

Předota M., Cummings P. T. and Wesolowski D. J. (2007b) Electric double layer at the rutile (110) surface. 3. Inhomogeneous viscosity and diffusivity measurement by computer simulations. *J. Phys. Chem. C* **111**, 3071–3079.

Předota M. and Vlček L. (2007a) Comment on parts 1 and 2 of the series ''Electric double layer at the rutile (110) surface''. *J. Phys. Chem. B* **111**, 1245–1247.

Předota M. and Vlček L. (2007b) Comment on parts 1 and 2 of the series ''Electric double layer at the rutile (110) surface''. *J. Phys. Chem. B* **111**, 1245–1247.

Předota M., Zhang Z., Fenter P., Wesolowski D. J. and Cummings P. T. (2004b) Electric double layer at the rutile (110) surface. 2. Adsorption of ions from molecular dynamics and X-ray experiments. *J. Phys. Chem. B* **108**, 12061–12072.

Ragnarsdottir K. V., Oelkers E. H., Sherman D. M. and Collins C. R. (1998) Aqueous speciation if yttrium at temperatures from 25 to 340 °C at P_{sat}: an in situ EXAFS study. *Chem. Geol.* **151**, 29–39.

Richens D. T. (1997) *The Chemistry of Aqua Ions*. Wiley-Interscience.

Ridley M. K., Hackley V. A. and Machesky M. L. (2006) Characterization and surface-reactivity of nanocrystalline anatase in aqueous solutions. *Langmuir* **22**, 10972–10982.

Ridley M. K., Machesky M. L., Palmer D. A. and Wesolowski D. J. (2002) Potentiometric studies of the rutile–water interface. Hydrogen-electrode concentration-cell vs glass-electrode titrations. *Colloids Surf. A: Physicochem. Eng. Aspects* **204**, 295–308.

Ridley M. K., Machesky M. L., Wesolowski D. J. and Palmer D. A. (1999a) Ca(II) adsorption at the rutile–water interface. A potentiometric study in NaCl media to 250 °C. *Geochem. Comochim. Acta* **63**, 3087–3096.

Ridley M. K., Machesky M. L., Wesolowski D. J. and Palmer D. A. (2004) Modeling the surface complexation of calcium at the rutile–water interface to 250 °C. *Geochem. Comochim. Acta* **68**, 239–251.

Ridley M. K., Machesky M. L., Wesolowski D. J. and Palmer D. A. (2005) Surface complexation of Neodymium at the rutile–water interface. A potentiometric and modeling study in NaCl media to 250 °C. *Geochim. Cosmochim. Acta* **69**, 63–81.

Ridley M. K., Palmer D. A., Wesolowski D. J. and Kettler R. M. (1998a) Cadmium malonate complexation in aqueous sodium trifluoromethanesulfonate media to 75 °C; including dissociation quotients of malonic acid. *J. Solut. Chem.* **27**, 195–216.

Ridley M. K., Palmer D. A., Wesolowski D. J. and Kettler R. M. (1998b) Potentiometric and solubility studies of aluminum malonate complexation in NaCl media to 75 °C. *Geochem. Comochim. Acta* **62**, 2279–2291.

Ridley M. K., Wesolowski D. J., Palmer D. A. and Kettler R. M. (1999b) Association quotients of aluminum sulphate complexes in NaCl media from 50 to 125 °C: results of a potentiometric and solubility study. *Geochem. Comochim. Acta* **63**, 459–472.

Rietra R. P. J. J., Hiemstra T. and Van Riemsdijk W. H. (1999) The relationship between molecular structure and ion adsorption on variable charged minerals. *Geochem. Comochim. Acta* **63**, 3009–3015.

Rietra R. P. J. J., Hiemstra T. and Van Riemsdijk W. H. (2001) Interaction between calcium and phosphate adsorption on goethite. *Environ. Sci. Technol.* **35**, 3369–3374.

Sahai N., Carroll S. A., Roberts S. and O'Day P. A. (2000) X-ray adsorption spectroscopy of strontium(II) coordination II. Sorption and precipitation at kaolinite, amorphous silica, and goethite surfaces. *J. Colloid Interf. Sci.* **222**, 198–212.

Seward T. M., Henderson C. M. B., Charnock J. M. and Driesner T. (1999) An EXAFS study of solvation and ion pairing in aqueous strontium solutions to 300 °C. *Geochim. Cosmochim. Acta* **63**, 2409–2418.

Stachowicz M., Hiemstra T. and van Riemsdijk W. H. (2006) Surface speciation of As(III) and As(V) in relation to charge distribution. *J. Colloid Interf. Sci.* **302**, 62–75.

Stern O. (1924) Zur theory der electrolytischen doppelschicht. *Z. Electrochem.* **30**, 508–516.

Stumm W. (1992) *Chemistry of the Solid–Water Interface*. John Wiley & Sons, Inc., New York, p. 428.

Sverjensky D. A. (2001) Interpretation and prediction of triple-layer model capacitances and the structure of the oxide–electrolyte–water interface. *Geochim. Cosmochim. Acta* **65**, 3643–3655.

Sverjensky D. A. (2005) Prediction of surface charge on oxides in salt solutions: revisions for 1:1 (M^+L^-) electrolytes. *Geochim. Cosmochim. Acta* **69**, 225–257.

Towle S. N., Bargar J. R., Brown, Jr., G. E. and Parks G. A. (1999a) Sorption of Co(II) on metal oxide surfaces II. Identification of Co(II)(aq) adsorption sites on the (0001) and (11#02) surfaces of a-Al_2O_3 by grazing-incidence XAFS spectroscopy. *J. Colloid Interf. Sci.* **217**, 312–321.

Towle S. N., Brown, Jr., G. E. and Parks G. A. (1999b) Sorption of Co(II) on metal oxide surfaces I. Identification of specific binding sites of Co(II) on (110) and (001) surfaces of TiO_2 (rutile) by grazing-incidence XAFS spectroscopy. *J. Colloid Interf. Sci.* **217**, 299–311.

Van Riemsdijk W. H. and Hiemstra T. (2006) The CD-MUSIC model as a framework for interpreting ion adsorption on metal(hydr)oxide surfaces. In *Surface Complexation* (ed. J. Luetzenkirchen). Elsevier.

Venema P., Hiemstra T. and Van Riemsdijk W. H. (1996a) Comparison of different site binding models for cation sorption: description of pH dependency, salt dependency, and cation–proton exchange. *J. Colloid Interf. Sci.* **181**, 45–59.

Venema P., Hiemstra T. and van Riemsdijk W. H. (1996b) Multisite adsorption of cadmium on goethite. *J. Colloid Interf. Sci.* **183**, 515–527.

Vlček L., Zhang Z., Machesky M. L., Fenter P., Rosenqvist J., Wesolowski D. J., Anovitz L. M., Předota M. and Cummings P. T. (2007) Electric double layer at metal oxide surfaces: static properties of the cassiterite–water interface. *Langmuir* **23**, 4928–4937.

Wesolowski D. J., Machesky M. L., Palmer D. A. and Anovitz L. M. (2000) Magnetite surface charge studies to 290 °C from in situ pH titrations. *Chem. Geol.* **167**, 193–229.

Westall J. and Hohl H. (1980) A comparision of electrostatic models for the oxide/soltuion interface. *Adv. Colloid Interface Sci.* **12**, 265–294.

Zhang Z., Fenter P., Cheng L., Sturchio N. C., Bedzyk M. J., Předota M., Bandura A., Kubicki J., Lvov S. N., Cummings P. T., Chialvo A. A., Ridley M. K., Bénézeth P., Anovitz L., Palmer D. A., Machesky M. L. and Wesolowski D. J. (2004) Ion adsorption at the rutile–water interface. Linking molecular and macroscopic properties. *Langmuir* **20**, 4954–4969.

Zhang Z., Fenter P., Kelly S. D., Catalano J. G., Bandura A. V., Kubicki J. D., Sofo J. O., Wesolowski D. J., Machesky M. L., Sturchio N. C. and Bedzyk M. J. (2006) Structure of hydrated Zn at the rutile TiO_2 (110)-aqueous solution interface. Comparison of X-ray standing wave, X-ray absorption spectroscopy, and density functional theory results. *Geochem. Comochim. Acta* **70**, 4039–4056.

Zhang Z., Fenter P., Sturchio N. C., Bedzyk M. J., Machesky M. L. and Wesolowski D. J. (2007) Structure of rutile TiO_2 (110) in water and 1 molal Rb^+ at pH 12: inter-relationship among surface charge, interfacial hydration structure, and substrate structural displacements. *Surf. Sci.* **601**, 1129–1143.

Associate editor: James Rustad